Tunable growth of gold nanostructures atÂ a PDMS surface to obtain plasmon rulers with enhanced optical features

Microchim Acta (2017) 184:3093–3102
DOI 10.1007/s00604-017-2323-z

ORIGINAL PAPER

Tunable growth of gold nanostructures at a PDMS surface to obtain plasmon rulers with enhanced optical features

Simona Scarano[1] · **Chiara Berlangieri**[1] · **Emiliano Carretti**[1] · **Luigi Dei**[1] · **Maria Minunni**[1]

Received: 27 January 2017 / Accepted: 3 May 2017 / Published online: 13 May 2017

Abstract Efficient coupling of plasmonic nanomaterials to optically transparent polymers still is a challenge in order to obtain affordable, versatile, and sensitive surface plasmonic devices. The in-situ fabrication of gold and silver nanoparticles on PDMS has been reported, but the resulting bulk sensitivities (of up to 70 nm RIU^{-1}) may still be improved. The authors report that few simple modifications to the general preparation of these composites (AuNPs@PDMS) can result in substantial improvements of the optical features. A two-steps growth of AuNPs@PDMS is found to be particularly effective. It includes chemical treatment of the PDMS surface before the formation of well-exposed and densely-packed 3D conglomerates of gold spheroids with enhanced bulk sensitivity. Differently from available approaches, the structures obtained by this method display sensitivity to refractive index change of about 250 nm per RIU. This is 3.5 times higher than spherical nanoparticles prepared by similar protocols and is near the optical performance of anisotropic NPs. Due to the strong 3D character of the structures, excellent plasmon coupling is realized on PDMS surface. The authors also show that these nanocomposite substrates can be subjected to external stimuli and then exhibit red shifts or blue shifts typical of induced plasmon coupling and uncoupling. Hence, the method represents a major step forward in terms of high-performance composite plasmonic nanomaterials for use in biosensing.

Keywords Localized surface plasmon resonance · Optical transducers · Polydimethylsiloxane · Biosensing · Nanostructures · Plasmon coupling · Bulk sensitivity

Introduction

The fabrication of plasmonic composite substrates for LSPR-based (bio)sensing has recently gained great attention, and cheap and versatile polymeric substrates such as polydimethylsiloxane (PDMS) for the in-situ growth of metal nanoparticles (mNPs) has been reported. These can be obtained by the spontaneous reduction of Au(III) or Ag(I) ions by simple immersion of cured PDMS films/blocks into metal salt solutions [1–6], without the need of additional reducing/capping agents. The formation of NPs at PDMS surface (hereafter NPs@PDMS) is attributed to residual curing agent present in the PDMS matrix after polymerization [4, 6, 7]. Gold and silver NPs formed at PDMS surface are generally spherical, with size and surface distribution depending on PDMS preparation (base monomer/curing agent ratio, η), Au(III) concentration ([Au]), and growth time. Afterward, cost and time consuming post-processing treatments such as thermal annealing and/or swelling/shrinking cycles are required to obtain final moderate refractive index sensitivity (RIS, ~70 nm RIU^{-1}). Until now, AuNPs@PDMS have been exploited for traditional LSPR biosensing, in which mNPs are further modified with bioreceptors (antibodies, nucleic acids *etc.*) targeting specific analytes [1–6], as well as for their direct testing upon external chemical/physical stimuli [8, 9]. The optical behavior of these substrates lead to the recording of red shifts of the NPs maximum wavelength (λ_{max}) and/or the absorbance intensity,

Electronic supplementary material The online version of this article (doi:10.1007/s00604-017-2323-z) contains supplementary material, which is available to authorized users.

✉ Simona Scarano
simona.scarano@unifi.it

[1] Department of Chemistry Ugo Schiff and CSGI, University of Florence, via della Lastruccia 3-13, Sesto Fiorentino, 50019 Florence, Italy

proportional to the concentration of the bound analyte and dielectric constant change at the near field [10]. The LSPR signal is hence the exclusive consequence of the NPs near field perturbation due to the biorecognition event occurring within its depth (in the order of few tens of nm). In fact, mean distances among NPs obtained by basic protocols exclude the contribution of inter-particle plasmon coupling. This phenomenon occurs only when mNPs are separated by short distances (from 1 to 2.5 folds their diameter), through the overlapping of their localized fields along dimer axis [11–14]. The overlapped near fields are characterized by extremely enhanced intensity, with obvious applicative advantages [15]. Under these conditions, the progressive shift of λ_{max} and/or band intensity is observed in a distance-dependent manner. Decrease of inter-particle separation leads to red shifts and enhanced intensity, whereas if NPs are pushed apart, a blue shift is recorded with loss in extinction peak intensity [16–19]. Therefore, the optical behavior can be directly related to mNPs distances in their environment. This band shift in the LSPR of coupled NPs found its nicest expression in the so-called plasmon rulers (PRs). This fascinating and emerging class of nanometrology devices is based on the exquisite, atomic-bond-length sensitivity to distance and their transduction of signal as a simple spectrophotometric measurement [19–22].

A two-steps growth of AuNPs@PDMS is here optimized, evidencing that PDMS surface chemical cleaning before the second growth is the key step in driving the formation of well-exposed and densely-packed 3D conglomerates of spheroids at the PDMS surface. These structures achieve sensitivity to refractive index change of about 250 nm RIU^{-1}. This value results about 360% higher than spherical nanoparticles prepared with similar protocols, and near the optical performances of anisotropic NPs. Due to the strong 3D character and near field intensity of the structures, the establishment of plasmon coupling effects among AuNPs is supposed. To confirm this assumption, plasmonically coupled or not AuNPs@PDMS substrates have been directly compared in their optical response through a classic immuno-based assay as reference approach. In fact, such a design performed on non-coupled AuNPs@PDMS leads only to red-shifted spectra. The local RI increment elicited by biomolecule binding at AuNPs surface is in fact the sole event occurring at the nanoscale. Conversely, coupled NPs subjected to the same biomodification react as plasmon rulers after protein absorption. As a consequence, the biofilm formed at the resonant nanostructured surface induces plasmon uncoupling. Typically, blue-shifted spectra and band intensity decrease are observed in this case.

The results here reported represent a step forward in understanding and controlling mNPs optical properties during their in-situ synthesis @PDMS surface, and represent a valid alternative to time and cost expensive existing approaches. A variety of applications from (bio)sensing to nanometrology can be envisaged, accounting for the design of new smart and cheap composite materials for nanophotonics. The whole AuNPs@PDMS fabrication process has been developed by modifying disposable UV-Vis cuvettes with PDMS films and then performing Au(III) reduction to NPs directly in-situ with the unique advantage of having a cheap, simple and highly stable composite substrates that can be interrogated by conventional spectrophotometry or portable spectrometers (Fig. 1).

Experimental section

Preparation of 'plasmonic' cuvettes

PDMS base monomer and curing agent (SYLGARD184 Silicone Elastomer kit, Dow Corning, Midland, MI, USA, https://www.dowcorning.com) were carefully weighted and thoroughly mixed in a weight proportion of 10:1, then degassed under vacuum for 20 min to eliminate air bubbles. Modification of UV-Vis cuvettes (Sigma-Aldrich, Milan, Italy, https://www.sigmaaldrich.com/italy.html) with PDMS was hence carried out as represented in Fig. S1A: a PDMS layer of 400 ± 20 μm was obtained keeping the cuvette lying on one of the two transparent sides and by casting known weight (35 mg) of the polymer on it. Borders were delimited by paper tape to confine the polymer into the cuvette. After deposition, the cuvette was placed in oven at 80 °C for 20 min. The procedure was repeated to modify the second transparent side of the cuvette. After PDMS coating, cuvettes were subjected to the in-situ growth of AuNPs@PDMS by incubation of aqueous $HAuCl_4$ (Sigma-Aldrich, Milan, Italy, https://www.sigmaaldrich.com/italy.html) at different concentrations for 96 h, sealed and in the dark at room temperature. To stop the AuNPs growth, Au(III) solutions were removed and cuvettes were washed three times with MilliQ water.

AuNPs@PDMS obtained from the first growth were subjected to a second growth with Au(III) solution to obtain plasmonically coupled nanostructures. To this aim, before the second growth, cuvettes are repeatedly washed with 96% ethanol. This treatment displayed the ability to tune the growth of plasmonically coupled AuNPs on the polymer surface during the second growth step. Substrates not subjected to ethanol washings were also prepared for comparison. Finally, cuvettes were dried under nitrogen flow and stored at 4 °C until use. Figure 1b reports the image of frontal and side view of the cuvettes.

Optical measurements

Extinction spectra of AuNPs@PDMS were recorded by a Perkin-Elmer Lambda 900 spectrophotometer. Refractive

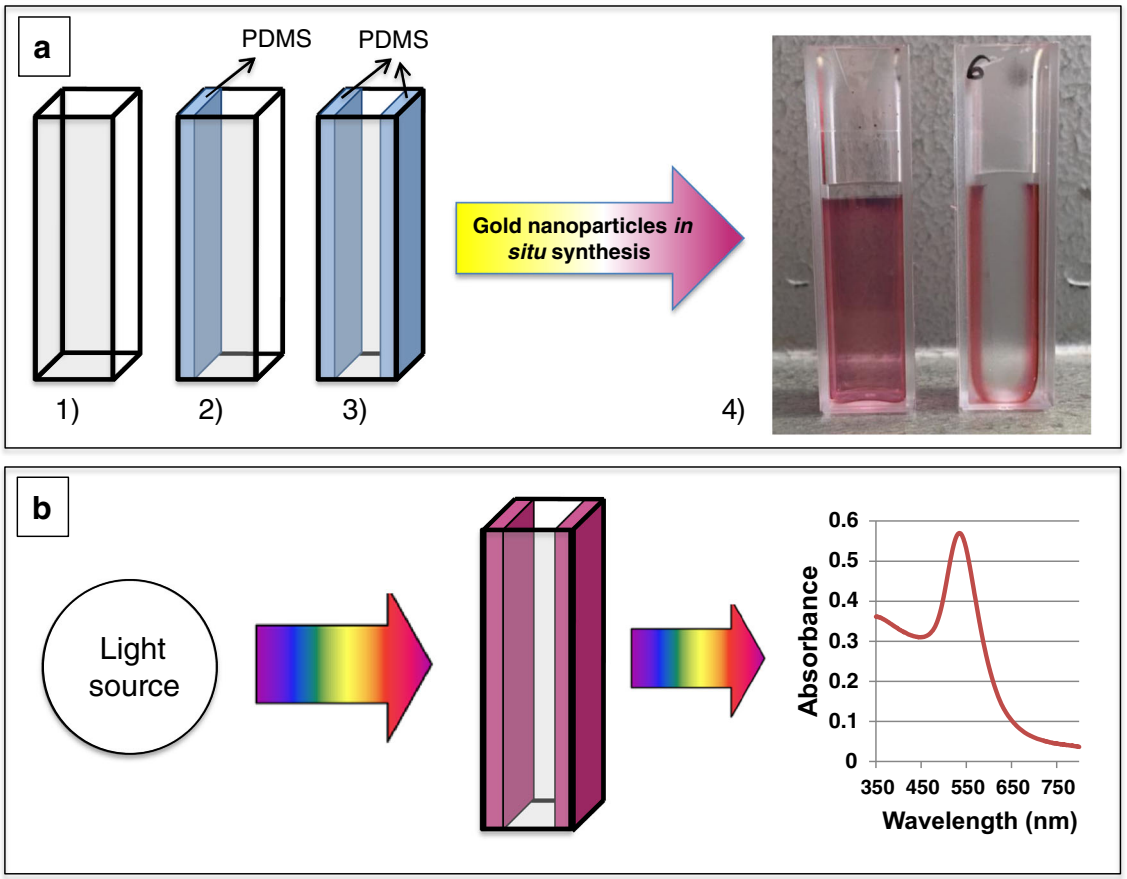

Fig. 1 **a** Sketched representation of 'photonic' cuvettes preparation. The transparent walls of disposable UV-Vis cuvettes (1) are coated with a PDMS layer (400 μm) in two steps (2–3). Then are filled with aqueous Au(III) solution at different concentrations and incubated for 96 h. Once the gold solution is removed, bright pale red color due to AuNPs formation is clearly evident by naked eye (4). **b** Optical interrogation of 'photonic' cuvettes is finally performed by classic spectrophotometry for LSPR measurements. The two modified walls both contribute to the LSPR reading as shown in the figure

index sensitivity (RIS) of substrates was tested in water-glycerol solutions by increasing the glycerol percentage from 0% to 70% with 10% steps. Non-modified cuvettes filled with the same solutions were tested to assess possible bulk contributions and baselines subtracted accordingly, if necessary. Before measurements, the modified cuvettes were treated several times by alternating ethanol/water washings, until stabilization of the plasmon band.

Extinction spectra were collected in the range 300–700 nm, with 1 nm resolution. RIS values were inferred from maximum wavelength shift (S_λ, nm RIU^{-1}) and/or absorbance intensity chance at fixed λ (S_{Abs}, a.u. RIU^{-1}), against refractive index unit change (RIU). $\Delta\lambda_{max}$ is the difference of the maximum absorbance wavelength (nm) recorded in glycerol solutions and water; ΔAbs is the difference of the absolute absorbance intensity (a.u.) at λ_{max} recorded under the same conditions. Δn is the corresponding variation of refractive index, i.e. $n_{glycerol}(\%) - n_{water}$. RI of deionized water was taken as 1.333.

Morphological analysis

The morphology of the substrates were investigated by Scanning electron microscopy (SEM). Images of PDMS layers modified with AuNPs were acquired by a FEI Quanta-200 ESEM at 25 kV. Mean size of AuNPs@PDMS surface were estimated by digital image analysis of SEM micrographies by ImageJ software (https://imagej.net/).

Bio-analytical assays

The optical behavior of the substrates was tested by an immuno-based assay. Chicken ovalbumin (100 μg mL^{-1} OVA, Sigma-Aldrich, Italy, https://www.sigmaaldrich.com/italy.html) was immobilized on AuNPs via spontaneous adsorption in saline phosphate buffer (0.1 M PBS, 0.1 M NaCl), and incubated 1 h at room temperature, then throughly washed with the same buffer prior recording spectral responses. To assess the saturation of AuNPs after

OVA immobilization, 400 μg mL^{-1} casein was subsequently incubated. Afterward, the binding of the specific antibody, i.e. anti-OVA IgG (Rockland Immunochemicals Inc., Tebu-bio, Milan, Italy, www.tebu-bio.com), was performed in cuvettes for 30 min, then the spectral variations were recorded in PBS. Regeneration of substrates was performed by short (2 min) washes of cuvettes with 10 mM NaOH. The regeneration step allowed the recovery of the initial λ_{max} and confirms the reversibility of the specific biorecognition.

Results and discussion.

Effect of [au(III)] on AuNPs@PDMS bulk sensitivity

The in-situ reduction of Au(III) on PDMS generally leads to spherical NPs of different size, distribution, and penetration depth as function of the curing agent to monomer ratio (η) [1–6]. In particular, Zhang et al. [6] investigated the influence of different η values at constant Au(III) concentration (25 mM). They found that the increase of curing agent (η > 0.1) leads to the formation of bigger particles well-exposed on the surface of the polymer. However, η = 0.1 is generally reported in literature, with [Au(III)] varying only between 0.5% and 2% (25–100 mM). Under these conditions, the obtained NPs display negligible RIS. Therefore, cost and time consuming post-processing treatments such as thermal annealing and/or swelling/shrinking cycles are required. Final substrates reach however only moderate RIS around 70 nm RIU^{-1}, likely ascribed to the growth of partially embedded AuNPs within the polymer bulk. Starting from these findings, we explored suitable modifications of the growth strategy to enhance the bulk sensitivity of these nanocomposites. To this aim, we tuned the formation of well-exposed AuNPs displaying plasmon coupling effects at the polymer surface. This in turn allows to enhance the RIS of the substrate. Differently from literature, for all the PDMS preparations, here the Au(III) concentration was changed keeping constant the η value (η = 0.1). The curing agent/[Au(III)] ratio (η', w mM^{-1}) was thus increased from 0.02 (1:50, 50 mM) up to 1 (1:1, 1 mM). Within the explored range, the substrates displayed a progressive change in color, gradually shifting from pale to purple red (Fig. 2a). Direct comparison of extinction spectra from the highest (50 mM, 'Type I') and the lowest (1 mM, 'Type II') Au(III) concentration shows a well defined peak centered at 537.5 ± 1.2 nm (n = 6, CV% 0.2) for Type I. This confirms fast reduction kinetics at high [Au(III)] (Fig. 2b). Contrarily, Type II is characterized by a broader and asymmetric extinction spectrum with λ_{max} = 565.6 ± 1.5 nm (n = 6, CV% 0.3). This is compatible with a slower growth rate which favors the formation of larger particles. SEM images support spectra behaviors and show that substrates differ for AuNPs density on PDMS surfaces. Therefore, gold concentration drives AuNPs growth both in terms of average particle size and distribution on the polymer surface.

Effect of PDMS thickness on AuNPs growth

PDMS thickness is also a key parameter to be taken into account: when lowered down to ~100 μm, the correlation between [Au(III)] and tunability of NPs is lost, and similar behaviors are obtained, despite from the initial [Au(III)]. This effect is likely related to the scarce availability of the reducing agent on the PDMS surface, which limits AuNPs growth. Spectra obtained from thin PDMS layers are characterized by a high and broad extinction band linearly increasing from red to blue wavelengths (Fig. S2). This is probably related to the observed partial loss of transparency of the modified PDMS. This additional finding indicates an important role of PDMS thickness in AuNPs@PDMS preparation.

Refractive index sensitivity after the first growth

The evaluation of refractive index sensitivity (RIS) is a common and informative way to estimate the susceptibility of localized plasmons toward refractive index changes in the surrounding medium [10]. Cuvettes modified with AuNPs@PDMS were therefore tested in water at increasing glycerol content (0–70%). Type I AuNPs@PDMS displayed a marked response of absorbance intensity change at fixed λ (S_{Abs} = 0.3170 ± 0.0007 a.u. RIU^{-1}), associated to the negligible presence of wavelength shift (S_λ < 10 nm RIU^{-1}) (Fig. S3). This behavior is sustained by the need of post-processing treatments of pristine AuNPs@PDMS (thermal annealing, plasma etching, swelling/shrinkage treatments, *etc.*) to enhance bulk sensitivity before their use for sensing purposes, as reported in literature [2–4, 6].

In fact, metallic NPs supported on solid substrates (e.g. glass or polymers) show a decrease of S_λ which is proportional to the NPs fraction volume in contact with the surface [23, 24]. Therefore, since PDMS surface is susceptible to local deformation of the polymeric network during AuNPs growth, the observed scarce S_λ bulk sensitivity of Type I indicates that NPs can be partially embedded into the polymer. Moreover, Au nanostructures densely distributed on solid substrates display a progressive disappearance of S_λ bulk sensitivity in favor of S_{Abs}. These kind of AuNPs thus express RIS prevalently by plasmon band intensity change rather than wavelength shift [25]. This is thus compatible with our morphological evaluation of Type I substrates.

On the contrary, Type II showed both absorbance intensity and maximum wavelength change. The absolute absorbance intensity of the peak at λ_{max} displayed a progressive change, well-described by an exponential fit (Fig. S4), corresponding to S_{Abs} of 0.2671 ± 0.0011 a.u. RIU^{-1}. The associated $\Delta\lambda_{max}$

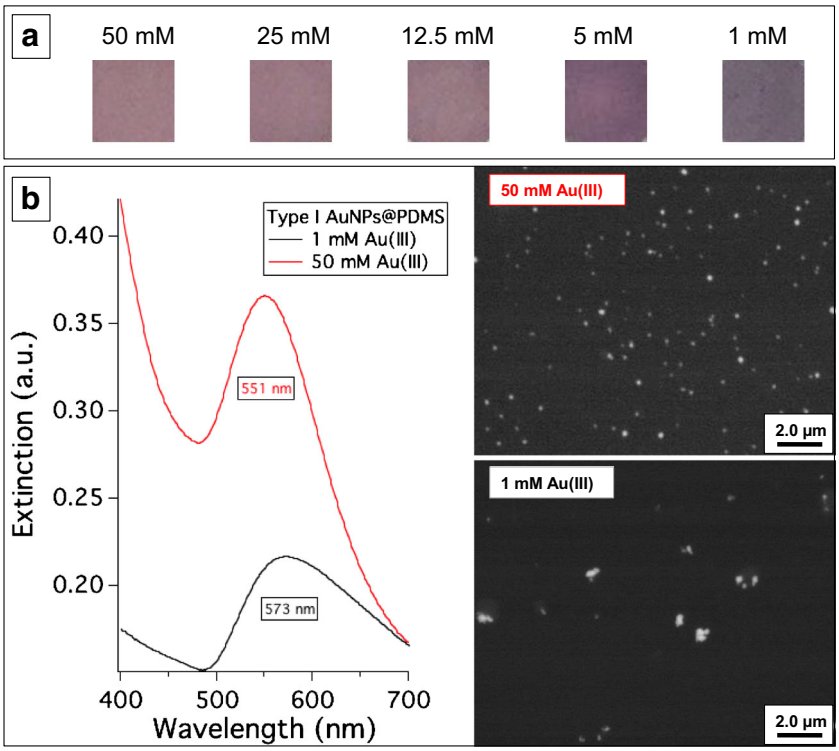

Fig. 2 **a** digital images of color change of AuNPs@PDMS by decreasing [Au(III)] from 50 mM to 1 mM. **b** extinction spectra and SEM images of AuNP@PDMS substrates relative to AuNPs prepared from 50 mM and 1 mM Au(III) for 96 h, hereafter named Type I and II

was 12 ± 1 nm within the whole RI interval, corresponding to $S = 126 \pm 10$ nm RIU^{-1}, with a linear correlation up to 1.40 RI (Fig. 3). This value is significantly higher than those reported in literature for similar composites (< 70 nm RIU^{-1}). The achievement is probably due to the combination of the high η' value used (η' = 1, i.e. curing agent:Au(III) ratio (w/mM)) respect to other approaches [3], and a longer growth time (96 h). The latter results indicate therefore that AuNPs@PDMS of Type II samples are well exposed over the PDMS surface and suitable for (bio)sensing applications.

In both the cases, the observed trend of absorbance intensity change is negative in terms of absolute change, but corresponds to the increase of the relative plasmon peak height, as expected as consequence of the refractive index increase (Fig. S5).

Inducing plasmon coupling by second growth

AuNPs are plasmonically coupled only if the inter-particle distance is comparable to their diameters [11–14]. Therefore, we attempted the tuning of AuNPs@PDMS to obtain the formation of proximal nanostructures to enhance the bulk sensitivity and to evidence plasmon coupling. To achieve the purpose, a second growth step on both Type I and II substrates (hereafter Type I^2 and Type II^2) was carried out. Cuvettes were subjected to ethanol washings before the addition of new Au(III) solution and its subsequent incubation. The target of ethanol treatment is the removal of residual surface curing/reducing agent after the first growth. This step is effective in obtaining different distributions of the nanostructures at PDMS surface. In case of ethanol treatment, the second growth of AuNPs is limited by the scarce availability of the reducing agent at the surface. Therefore, substrates subjected to ethanol treatment between growths show large particles at low density (Fig. S6). Contrarily, if ethanol treatment is avoided, particles appear smaller and more homogeneously-distributed over the polymer surface. Spectra of Type I^2 samples (Fig. S7) confirm SEM images. In absence of ethanol treatment the plasmon peak results significantly higher and narrow, with $\lambda_{max} = 535.3 \pm 1.1$ nm. On the contrary, when the treatment is performed the peak is lower, broad, and red-shifted to 542 nm (Fig. S7). This trend is more evident in case of Type II^2 substrate. The relative spectrum is well-compatible with NPs clustering, since a large red shift from 565.6 ± 1.5 to 648.3 ± 8.4 nm along with a marked absorbance intensity enhancement is observed (Fig. S8). The averaged dimensions of Au clusters have been evaluated from SEM micrographs, and image analysis supports the spectral behaviors. In particular, the estimated average size of nanostructures resulted around 120 nm and 200 nm for Type I^2 and Type II^2 respectively (Fig. S9). The substrates differ also for AuNPs density on PDMS surface and size distribution. In case of Type II^2 the analysis shows a wider dispersion of particle size, in accord to the prevalence of metallic clusters at the surface.

The morphological differentiation is particularly evident on Type II substrates, displaying densely-packed sub-micrometer conglomerates after ethanol treatment. This morphology is likely the result of a fine interplay between kinetics and thermodynamics of underlying nucleation and growth on the first

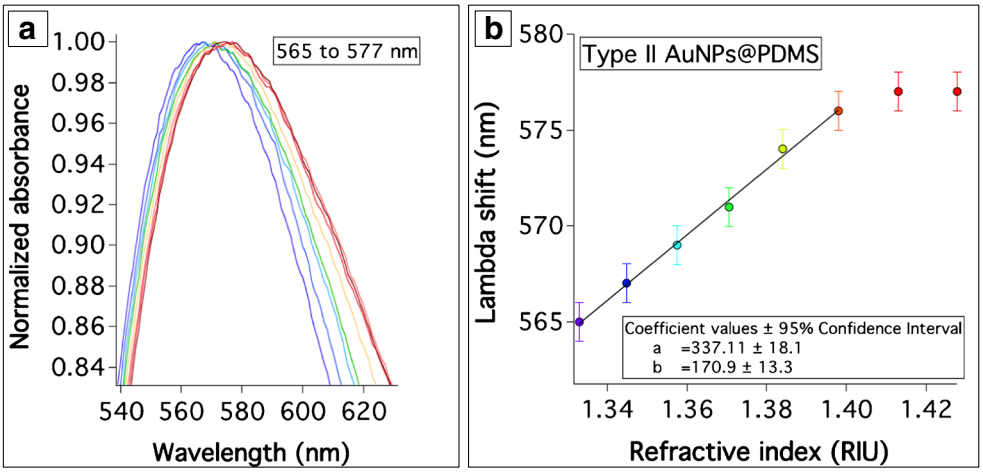

Fig. 3 **a** Transmission spectra recorded at different glycerol % in water (0–70%). RI sensitivity of Type II AuNPs@PDMS is evidenced as maximum wavelength red shift (S_λ), with an overall $\Delta\lambda_{max}$ = 12 nm. **b** Plot of the linear correlation between $\Delta\lambda_{max}$ and Δn, where S_λ is obtained as $\Delta\lambda_{max}/\Delta n$ ratio. Standard deviations are obtained from independent measurements on the same cuvette (n = 3)

AuNPs generation. However, as it can be observed by Fig. 4a, NPs composing the conglomerates have roughly comparable size and shape. Therefore, we can hypothesize that the large red-shift and intensity increase observed for Type II^2 can be prevalently ascribed to plasmon coupling effects among proximal NPs on the surface. This is in agreement not only with NPs densely packed and well exposed toward the bulk [25], but also with the enhancing effect elicited by the near field overlapping. The RIS of both substrates has been evaluated. Type I^2 samples did not display RIS increase in terms of S_λ (Fig. S10), but only in terms of S_{Abs}, from 0.3170 to 0.3725 ± 0.0017 a.u. RIU^{-1}. Contrarily, the S_λ of Type II^2 resulted greatly improved compared to the first growth (Fig. 4b-d), whereas the associated S_{Abs} increased only from 0.2671 to 0.2887 ± 0.0032 a.u. RIU^{-1}.

In particular, within the RI change associated to the binding of the biomolecules on mNPs, NPs are characterized by an enhancement of more than 200% the initial sensitivity, i.e. 254 ± 11 nm RIU^{-1} (Δn = 1.3448–1.3330, Fig. 4d). The obtained sensitivity is also noticeably higher than those obtained by classic spherical NPs supported on solid/polymeric surfaces (~70 nm RIU^{-1}). In particular, it results similar to sensitivities of pre-formed nanostars immobilized on PDMS via silanization [26]. Attempts in obtaining in-situ growth of non-spherical AuNPs@PDMS are still limited [27] and deserve to be improved. Therefore, these results represent a step forward in fabricating sensitive plasmonic nanostructures without the need of post-processing treatments.

Behavior of AuNPs@PDMS as plasmon rulers

To verify that Type II^2 substrates support plasmon coupling among AuNPs, we directly compared the optical behavior of the two nanocomposites (Type I^2 and Type II^2) through a classic immuno-based assay. As proof-of-principle test, we used ovalbumin (OVA) as antigen and anti-ovalbumin antibody (anti-OVA) as specific antibody for its biorecognition. This with perspective application of the approach to the identification of egg proteins on artwork surfaces by optical biosensing, as recently reported [28]. The rationale is that such a design performed by plasmonic substrates in which coupling effects are negligible, i.e. Type I^2 in this case, leads only to red-shifted spectra. This effect is due to the local RI increment elicited by biomolecule binding at AuNPs surface, that is the sole event occurring at the nanoscale. Conversely, coupled NPs subjected to the same biomodification may act as plasmon rulers [16–22] after protein absorption. This is due to the formation of a biofilm at the nanostructured surface which may cause steric hindrance, plasmon uncoupling, and related blue-shifted spectra of lower intensity. Therefore, the adsorption of OVA (100 μg mL^{-1}) on Types I^2 and II^2 AuNPs@PDMS followed by buffer washing to eliminate unbound protein is carried out. Accordingly to previous findings and considerations on Type II^2 substrate, a marked blue-shift from 648 nm to 605 nm occurred, whereas Type I^2 showed a classical (from 543 to 547 nm) red shift (Fig. 5a).

These results confirm that, depending on their own features, Type II^2 AuNPs@PDMS may act as stimuli-responsive nanomaterial. In particular, it can be assumed that the protein diameter (5.4 nm) is small enough to penetrate in interstitial spaces among AuNPs conglomerates and elicit mesospacing variation, evidenced by the characteristic blue shift, as sketched in Fig. 5a (right). Furthermore, the expected decrease of extinction intensity (Fig. S11) sustains the plasmon ruler behavior and is associated to inter-particle distance increase induced by protein binding. Contrarily, on Type I^2 OVA adsorption induces a red shift, which is well-compatible with a classical LSPR-based biosensing. This can be accounted by the absence of plasmon coupling among NPs at the surface (Fig. 5a).

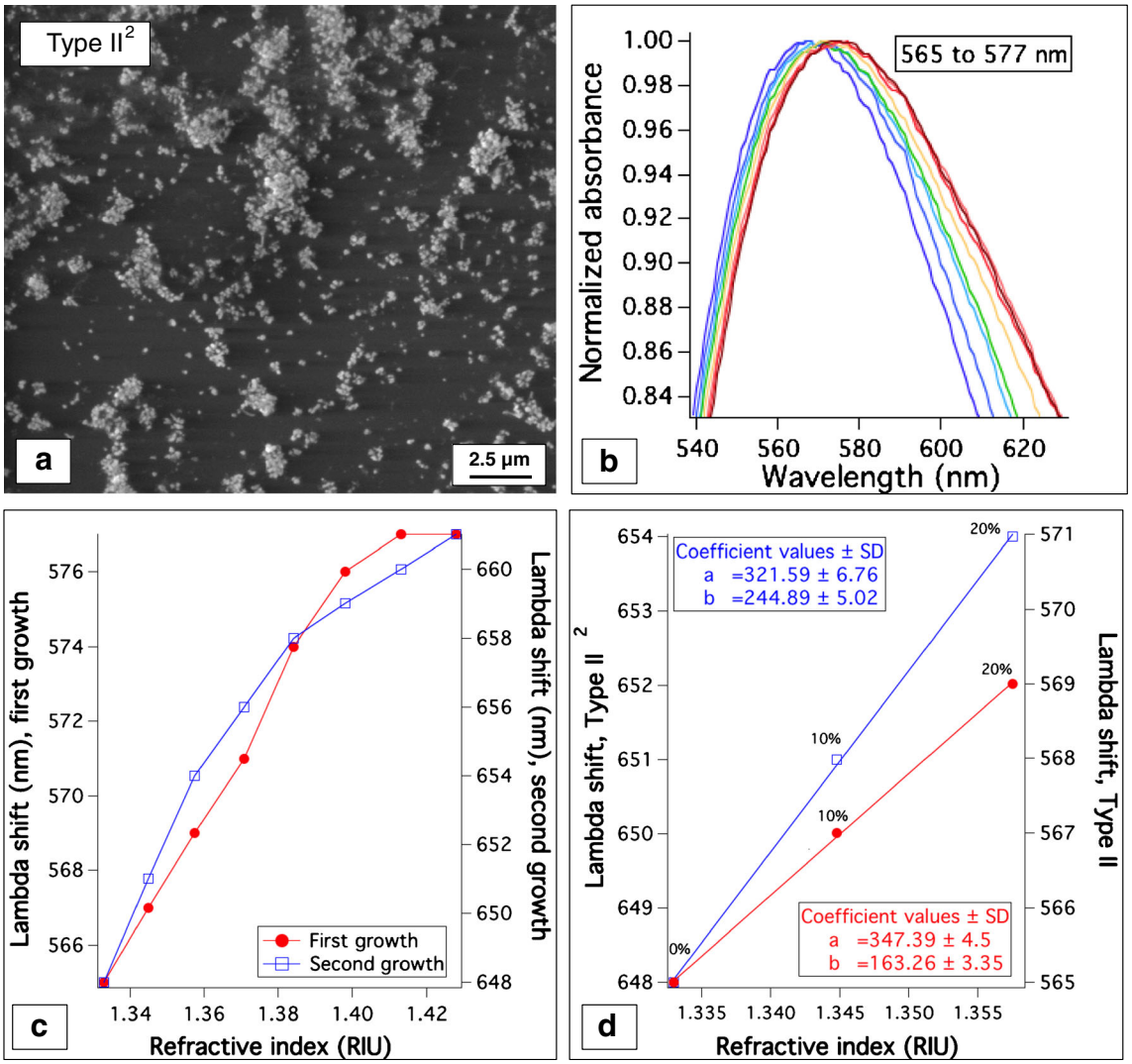

Fig. 4 **a** SEM image of Type II² AuNPs@PDMS when ethanol treatment is performed between the two growths. The 3D sub-micrometer AuNPs clusters are clearly visible at the polymer surface; **b** transmission spectra of Type II² showing λ_{max} shift with RI increase (0–70% glycerol); **c** comparison of λ_{max} shifts obtained on Type II (*red*) and Type II² (*blue*) substrates; **d** Zoom in of the RIU range of interest for biomolecular interaction studies

To further sustain this assumption, anti-OVA (1 μg mL^{-1}) was incubated on the adsorbed OVA on both substrates. After a saturation step with casein and washing with buffer, the spectral response of the substrates was compared. Interestingly, the binding of the antibody is able to induce red-shifted spectra in both cases (Fig. 5b-c). In particular, the marked red shift recorded on Type II² (6 nm) is strongly informative of a classic LSPR response. It clearly indicates that the antibody prevalently binds the exposed surface of the immobilized OVA, but it does not induce further plasmon uncoupling among NPs. This finds further confirmation in the opposite variation of absorbance intensity, i.e. an intense (0.04 a.u.) increase instead of the decrease recorded during OVA immobilization (Fig. S12). The result is coherent with data elsewhere reported for bovine serum albumin binding by classic molecular LSPR reading, in which antibody binding elicits the expected intensity increase [29, 30]. After anti-OVA binding, a brief (2 min) treatment with 10 mM NaOH is able to regenerate the biochip surface and to recover the starting wavelength and intensity recorded before anti-OVA interaction (data not shown). As expected from data obtained on its bulk sensitivity, Type I² demonstrated scarce near-field sensitivity to anti-OVA binding in terms of λ_{max}. This result supports that AuNPs@PDMS require dedicated post-treatments to enhance the S_λ [2–4, 6].

As a whole, Type II² substrates display not only excellent bulk sensitivity (>250 nm RIU^{-1}) respect to the available literature (~70 nm RIU^{-1}), but also the specialized ability in sensing mesospacing variation at the nanoscale upon external stimulus. Moreover, the specific biorecognition of the adsorbed protein can be further performed by classical

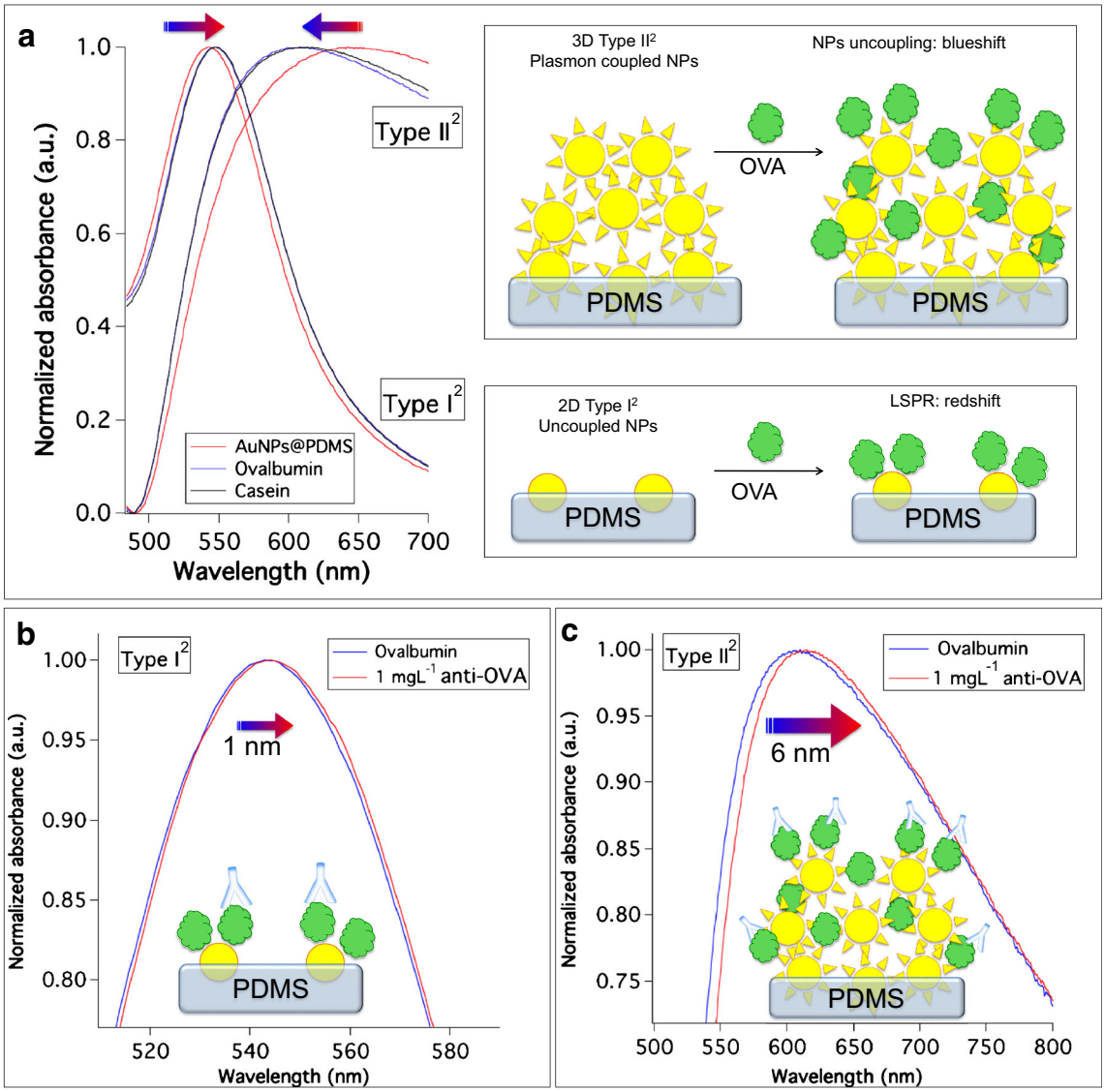

Fig. 5 **a** Spectra of Type I^2 and Type II^2, in which the opposite behavior of the two substrates is directly compared after ovalbumin (OVA) adsorption and casein saturation. Plasmonically coupled substrate, Type II^2, displays a marked *blue shift* whereas Type I^2, in which this feature is absent, shows the classical red shift. On the right, sketched representations of the two different optical effects induced by OVA adsorption. **b**, **c**) *Red shifts* induced by the specific binding of anti-OVA IgG on Type I^2 and Type II^2, respectively. In this case both substrates react with a *red shift* of the wavelength, marked for Type II^2 as consequence of plasmon coupling at the surface

LSPR, distinguishing the recognition step from the former by the opposite blue/red spectral shift.

Classical LSPR measurements on AuNPs immobilized on glass after their modification with Bovine serum albumin (BSA) at the same concentration give up to ~30 nm of λ_{max} shifts at the saturation point of the sensor [29]. Therefore, as preliminary evaluation, the sensitivity of Type II^2 results roughly 2.5 folds higher in terms of λ_{max} shift (80 ± 3 nm). A remarkable gain of signal is also obtained in terms of absorbance intensity change (ΔAbs (10^{-2}) = 4 a.u.). This variation is about one order of magnitude higher respect to the response obtained through immuno-based albumin recognition by classical substrate preparation (pre-formed AuNPs immobilized on glass) [30].

It should be noted that the structures used in these experiments have not yet been optimized to obtain the lowest limits of detection, but already demonstrate that these substrates can display enhanced analytical performances. Moreover, they are able to differentiate molecular interactions from bulk index changes at the metallic surface.

Conclusions

Spherical AuNPs@PDMS obtained by available protocols display intrinsic RI sensitivity below 70 nm RIU^{-1}. This limits their use in LSPR-based applications at the forefront of the research. Herein we investigated the

possibility to tune and enhance the optical performance of AuNPs@PDMS composites. This goal has been pursued by avoiding long and expensive post-processing treatments, and by playing only on the synthetic route. We showed that there is room for new approaches in controlling morphology and functioning of these smart and promising stimuli-responsive materials. The intriguing finding is that low Au(III) concentration (1 mM) coupled to an extended growth time (96 h) is a key strategy to favor the growth of large and well-exposed spherical AuNPs with improved sensitivity (>120 nm RIU^{-1}). The use of high (50 mM) or low (1 mM) Au(III) concentration deeply influences the RIS observed. In the first case, a predominant absorbance-dominated RIS is obtained, whereas low Au(III) availability produces larger nanostructures dominated by scattering phenomena. The flexibility and the partial permeability of PDMS to Au(III) gold solution during NPs growth has to be taken into account. In fact, high [Au(III)] induces the growth of AuNPs with scarce RIS, as also reported by other authors. The reproducibility and the stability of the substrates strongly depend on their preparation, e.g. PDMS thickness and batch-to-batch variation of Au(III) solutions. The removal of the reducing agent at the PDMS surface can strongly modulate the morphology of the new generation of AuNPs during a second growth step. In particular, it triggers the appearance of well-exposed 3D conglomerates characterized by a strong enhancement of the bulk sensitivity (>250 nm RIU^{-1}) due to plasmon coupling effects at the surface. The molecular sensitivity of these substrates results significantly enhanced compared to classical AuNPs immobilized on glass substrates, both in terms of wavelength and absorbance shift.

These nanocomposite materials represent therefore a fruitful direction accounting for the design of new smart substrates to be applied to (bio)sensing. Further work can be done in the direction of controlling morphology and function of these promising stimuli-responsive materials, to obtain the controlled in-situ growth of anisotropic NPs expressing different spectral fingerprints to be used in microarray format. We foresee the rational use of these substrates as plasmon rulers for nanometrology, an exciting and emerging topic of broad interest in different fields. Plasmon rulers represent a challenging tool to achieve the precise measurement of distance variations, down to few tens of Ångstroms, by exploiting the plasmon coupling/uncoupling dynamics.

Acknowledgements The authors thank the Ministry of Education, University and Research (MIUR) for the scientific program SIR2014 Scientific Independence of young Researchers (RBSI1455LK).

Compliance with ethical standards The author(s) declare that they have no competing interests.

References

1. Dunklin JR, Forcherio GT, Berry KR Jr, Roper DK (2013) Asymmetric reduction of gold nanoparticles into Thermoplasmonic polydimethylsiloxane thin films. ACS Appl Mater Interfaces 5:8457–8466. doi:10.1021/am4018785
2. Ozhikandathil J, Badilescu S, Packirisamy M (2012) Gold nanostructure-integrated silica-on-silicon waveguide for the detection of antibiotics. In milk and milk products. Proceedings of SPIE, photonics north conference, 800707
3. Sad Abadi H, Badilescu S, Packirisamy M, Wüthrich R (2012) PDMS-gold nanocomposite platforms with enhanced sensing properties. J Biomed Nanotechnol 8:539–549. doi:10.1166/jbn.2012.1418
4. Sad Abadi H, Badilescu S, Packirisamy M, Wüthrich R (2013) Integration of gold nanoparticles in PDMS microfluidics for lab-on-a-chip plasmonic biosensing of growth hormones. Biosens Bioelectron 44:77–84. doi:10.1016/j.bios.2013.01.016
5. Wu WY, Bian ZP, Wang W, Zhu JJ (2010) PDMS gold nanoparticle composite film-based silver enhanced colorimetric detection of cardiac troponin. Sens Actuator B-Chem 147:298–303. doi:10.1016/j.snb.2010.03.027
6. Zhang Q, Xu JJ, Liu Y, Chen HY (2008) In-situ synthesis of poly(-dimethylsiloxane)-gold nanoparticles composite films and its application in microfluidic systems. Lab Chip 8:352–357. doi:10.1039/b716295m
7. Goyal A, Kumar A, Patra PK, Mahendra S, Tabatabaei S, Alvarez PJJ, John G, Ajayan PM (2009) In situ synthesis of metal nanoparticle embedded free standing multifunctional PDMS films. Macromol. Rapid Commun 30:1116–1122. doi:10.1002/marc.200900174
8. Li X, Gao Y, Serpe M (2016) Stimuli-responsive polymers and their applications. Gels 2:8–28. doi:10.1039/C6PY01585A
9. Cataldi U, Caputo R, Kurylyak Y, Klein G, Chekini M, Umeton C, Bürgi T (2014) Growing gold nanoparticles on a Flexible substrate to enable simple mechanical control of their Plasmonic coupling. J Mater Chem C 37:7927–7933. doi:10.1039/C4TC01607F
10. Szunerits S, Boukherroub R (2012) Sensing using localised surface Plasmon resonance sensors. Chem Commun 48:8999–9010. doi:10.1039/C2CC33266C
11. Maier SA, Brongersma ML, Kik PG, Atwater HA (2002) Observation of near-field coupling in metal nanoparticle chains using far-field polarization spectroscopy. Phys. Rev. B: Condens. Matter Mater. Phys 65:193408. doi:10.1103/PhysRevB.65.193408
12. Rechberger W, Hohenau A, Leitner A, Krenn JR, Lamprecht B, Aussenegg FR (2003) Optical properties of two interacting gold nanoparticles. Opt Commun 220:137–141. doi:10.1016/S0030-4018(03)01357-9
13. Nordlander P, Oubre C, Prodan E, Li K, Stockman MI (2004) Plasmon hybridization in nanoparticle dimers. Nano Lett 4:899–903. doi:10.1021/nl049681c
14. Su KH, Wei QH, Zhang X, Mock JJ, Smith DR, Schultz S (2003) Interparticle coupling effects on Plasmon resonances of Nanogold particles. Nano Lett 3:1087–1090. doi:10.1021/nl034197f
15. Guo L, Jackman JA, Yang HH, Chen P, Cho NJ, Kim DH (2015) Strategies for enhancing the sensitivity of Plasmonic nanosensors. Nano Today 10:213–239. doi:10.2217/nnm.09.48
16. Sönnichsen C, Reinhard BM, Liphardt J, Alivisatos AP (2005) A molecular ruler based on Plasmon coupling of single gold and silver nanoparticles. Nat Biotechnol 23:741–745. doi:10.1038/nbt1100
17. Jiang N, Ruan Q, Qin F, Wang J, Lin HQ (2015) Switching Plasmon coupling through the formation of dimers from polyaniline-coated gold Nanospheres. Nano 7:12516–12526. doi:10.1039/C5NR02619

18. Mahmoud MA (2015) Polarized Optomechanical response of silver Nanodisc monolayers on an elastic substrate induced by stretching. J Phys Chem C 119:19359–19366. doi:10.1021/acs.jpcc.5b05359
19. Mahmoud MA (2016) Silver Nanodisk monolayers with surface coverage gradients for use as optical rulers and protractors. Langmuir 32:11631–11638. doi:10.1021/acs.langmuir.6b03211
20. Hill RT, Mock JJ, Hucknall A, Wolter SD, Jokerst NM, Smith DR, Chilkoti A (2012) Plasmon ruler with angstrom length resolution. ACS Nano 6:9237–9246. doi:10.1021/nn3035809
21. Chen T, Hong Y, Reinhard BM (2015) Probing DNA stiffness through optical fluctuation analysis of Plasmon rulers. Nano Lett 15:5349–5357. doi:10.1021/acs.nanolett.5b01725
22. Lee SE, Chen Q, Bhat R, Petkiewicz S, Smith JM, Ferry VE, Correia AL, Alivisatos P, Bissell MJ (2015) Reversible aptamer-au Plasmon rulers for secreted single molecules. Nano Lett 15:4564–4570. doi:10.1021/acs.nanolett.5b01161
23. Martinsson E, Shahjamali MM, Large N, Zaraee N, Zhou Y, Schatz GC, Mirkin CA, Aili D (2016) Influence of surfactant bilayers on the refractive index sensitivity and catalytic properties of anisotropic gold nanoparticles. Small 12:330–342. doi:10.1002/smll.201502449
24. Martinsson E, Otte MA, Shahjamali MM, Sepulveda B, Aili D (2014) Substrate effect on the refractive index sensitivity of silver nanoparticles. J Phys Chem C 118:24680–24687. doi:10.1021/jp5084086
25. Tesler AB, Chuntonov L, Karakouz T, Bendikov TA, Haran G, Vaskevich A, Rubinstein I (2011) Tunable localized plasmon transducers prepared by thermal dewetting of percolated evaporated gold films. J Phys Chem C 115:24642–24652. doi:10.1021/jp209114j
26. Shiohara A, Langer J, Polavarapu L, Liz-Marzán LM (2014) Solution processed polydimethylsiloxane/gold Nanostar Flexible substrates for plasmonic sensing. Nano 6:9817–9823. doi:10.1039/c4nr02648a
27. Chekini M, Cataldi U, Maroni P, Guénée L, Černý R, Bürgi T (2015) Preparation of anisotropic and oriented particles on a Flexible substrate. Langmuir 31:13221–13229. doi:10.1021/acs.langmuir.5b03524
28. Scarano S, Carretti E, Dei L, Baglioni P, Minunni M (2016) Coupling non invasive and fast sampling of proteins from work of art surfaces to surface Plasmon resonance Biosensing: differential and simultaneous detection of egg components for cultural heritage diagnosis and conservation. Biosens Bioelectron 85:83–89. doi:10.1016/j.bios.2016.04.093
29. Jia K, Khaywah MY, Li Y, Bijeon JL, Adam PM, Déturche R, Guelorget B, François M, Louarn G, Ionescu RE (2013) Strong improvements of localized surface plasmon resonance sensitivity by using au/ag bimetallic nanostructures modified with polydopamine films. ACS Appl Mater Interfaces 6:219–227. doi:10.1021/am403943q
30. Fujiwara K, Watarai H, Itoh H, Nakahama E, Ogawa N (2006) Measurement of antibody binding to protein immobilized on gold nanoparticles by localized surface plasmon spectroscopy. Anal Bioanal Chem 386:639–644. doi:10.1007/s00216-006-0559-2